EFFECT OF SHOT PEENING PROCESS ON ROLLING CONTACT FATIGUE PERFORMANCE OF EN 31 ALLOY STEEL

Ranju M.R* and D. Kesavan

Department of Mechanical Engineering

Indian Institute of Technology, Palakkad, Kerala, India- 678623

Corresponding author: Ranju M.R (ranjumankara7@gmail.com)

ABSTRACT

This paper aims to study the effect of shot peening on the Rolling Contact Fatigue (RCF) life of EN 31 Steel subjected to a pure rolling condition. Tests were carried out under lubricated contact conditions using a two-disc on-cylinder test rig. The orthogonal stress distributions and depth of deformation zones under static loading conditions were calculated using an elastic model by Finite Element Analysis (FEA) method. Shot peening increased the surface hardness by 20 % and imparted residual stress, which resulted in a 2-fold improvement of life. The depth of origin of the crack from the sub-surface was found to be in good agreement with the depth of maximum shear region obtained from the finite element model.

Keywords: Rolling contact fatigue, Shot peening, Subsurface crack, RCF life

Introduction

Rolling contact fatigue (RCF) failure is evidenced as a material flaking type of failure majorly observed in bearings, gears, and rail wheels. This type of failure arose due to the high intensity of localized stress results when two curved surfaces or non-conformal surfaces which are in contact, acted upon a normal load. This state of stress is generally called the Hertzian state of stress and forms a small volume of elliptical contact stress region within the material [1–5]. There are two predominant mechanisms observed in the case of RCF failures, they are, surface originated spalling and subsurface originated pitting. These modes of failures are depending on a number of factors such as surface quality, lubricant properties and material cleanliness [6].

Bearings are the major components experiencing sub surface-initiated failures due to repeated contact load during the operation. Most subsurface cracks originate from the sub surface inclusions, which act as the dislocation accumulation point and induce microplastic strain in it [7]. Different hardening techniques are used to improve the rolling contact fatigue performance of the bearing steels. Shot peening is one among the mechanical surface treatment processes widely used in aerospace industries to improve fatigue performance [8]. Shot peening is a high strain rate method that produces high plastic deformation on a target surface by bombarding small hard particles at high velocity on it [9]. Compressive residual stress, increased surface hardness and surface roughness are the major outcomes of this process [10,11]. Dynamic and static

strain ageing resulting from the shot peening will decrease the dislocation mobility. Further deformation during the process causes dislocation multiplication and induces a compressive residual stress [10]. The enhancement of fatigue life and reliability of the machine components are the major focus of this treatment [12,13][14]. Since the EN-31 steel is frequently used for bearing surfaces, it is sometimes referred to as bearing steel. This study investigates the effect of shot peening on the rolling contact fatigue life of EN 31 alloy steel by using a twin disc-on-cylinder test rig. FEA analysis for the same contact is performed and analysed the surface and subsurface shear stress distribution.

EXPERIMENTAL AND COMPUTATIONAL DETAILS

Materials and methods

Forged steel of EN 31 grade is subjected to rough machining followed by thermal treatment and finally a superfinishing process is performed to achieve the desired surface finish and hardness is used for the test. The elemental composition of the material is tabulated below in Table 1. The steel sample is hardened by homogenisation at 870°C for 20 minutes, followed by quenching and ageing for 120 minutes to get the required structure and hardness. The heat-treated sample is taken for a fine turning and then lapping process for 15 minutes by using 0.5 - 1 μm diamond paste and velvet cloth. This process is done manually by fixing the sample in a lathe at a lower speed

Table 1: Chemical composition (in wt.%) of EN31 grade steel

Element	C	Si	Mn	Cr	Ni	Cu	Fe
Weight (%)	1.18	0.30	0.34	1.52	0.03	0.007	balance
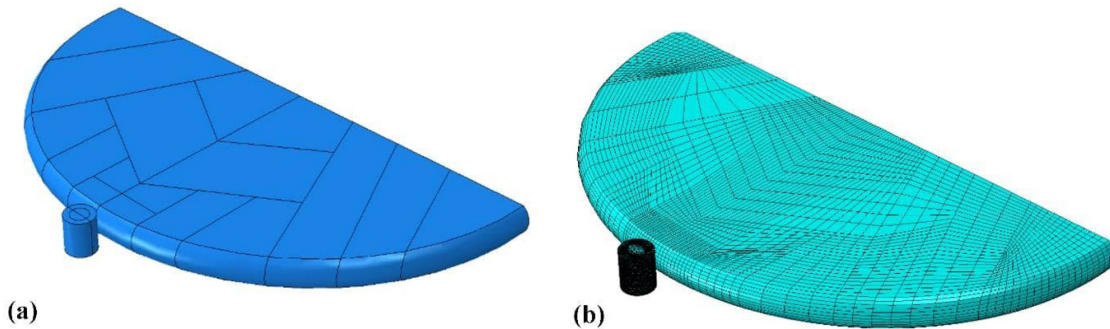
Fig. 1. (a) 3D contact model and (b) Meshing details of the model

range of 700 - 1000 rpm. Soon after the lapping, a set of specimens is taken for a shot peening process by using S17 cast steel balls of 0.4 mm diameter. Different duration of shot peening is considered for comparison.

Material characterisation

The specimens are taken for surface analysis to evaluate the surface roughness and profile changes. This analysis is performed under an optical non-contact profilometer (NanoMap 1000WLI). The cross section of the specimen is taken for surface and subsurface hardness analysis by using micro hardness tester (AFFRI model 251 VRSA) with a load of 10 kg and 10 sec dwell time. After RCF testing, the samples were cut in a plane parallel to the contact wear track and polished with a diamond paste of 0.4 μm to see the subsurface morphology. The subsurface crack analysis is performed with scanning electron microscopy (Zeiss Gemini SEM-300).

Finite Element Modelling

FE modelling is done to understand the surface and subsurface stress distribution in the contact. The model consists of a deformable disc of diameter 180 mm and cylindrical rod of 10 mm diameter. The present model developed takes the advantages from symmetries and ignores the regions far from the contact with very less to no stress. This model consists of two parts: one is the top half of the disc and the other one is a cylindrical rod. A symmetry boundary condition is applied on the top half of the roller. The other half of the model was ignored in the model because of negligible stress. The rod was radially loaded by a single disc for reducing computation time, whereas a two-disc test rig was used in the actual experimental setup. Modern bearings are well lubricated with low friction coefficient between rolling elements. Considering this as an assumption a frictionless contact was defined at the contact interfaces between the disc and cylindrical rod. The cylindrical rod is loaded by a single roller with the radial load of 1.3 kN. Using the interaction module in Abaqus, the contact interaction between the bottom surface of the disc and the top surface of the

cylindrical specimen are defined. General contact algorithm is used for this study. This is defined for a surface pair viz., the top surface of the specimen and the bottom surface of the disc based on the user guidelines from Abaqus[15]. Under the 'normal behavior' property selection, a "Hard" contact condition is adapted from the given options in Abaqus. Usually, this contact condition is used to minimize the penetration of the slave surface into the master surface at the contact locations and does not allow the transfer of tensile stress across the interface. The cylindrical rod is meshed with a total of 827680 elements. To accurately capture the contact stress, a fine mesh has been adopted in the vicinity of Hertzian contact shown in Fig. 1. Quadratic hexahedral elements of type C3D20 (20 node brick element) were used at the region of contact to predict the stress accurately. The region other than that of the contact was meshed with a linear hexahedral element C3D8 (8 node brick element). On the other hand, roller was modelled as an isotropic material with elastic response material using E = 210 GPa and disc was also meshed with both C3D20 as well as C3D8 elements.

Analytical studies of contact stress

Formulas for principal stresses at the contact and the variation of stresses at the sub-surfaces of the contacting surfaces are taken from the K L Johnson model [16]. When two non-conforming convex elastic bodies are brought into contact and applied with the normal load will deform the surfaces to form an elliptical contact region, with major and minor axes being 'a' and 'b' respectively.

Contact pressure calculation:

Maximum contact pressure at the elliptical contact region is given by,

$$P_{max} = \frac{1}{\pi} \left(\frac{6wE^{*2}}{R_e{}^2} \right)^{\frac{1}{3}} \tag{1}$$

Where,
W = Applied load in kN
E^* = Compound modulus (kN/mm²)

$$\frac{1}{E^*} = \left[\frac{1-v_1^2}{E_1} + \frac{1-v_2^2}{E_2}\right]$$

v = Poisson's ratio = 0.3
R_e = Effective or equivalent contact radius.
c = Mean contact radius

Shear stress calculation

The stresses along the z-axis can be calculated by using the relation given in [16].

Shear stress is given by.

$$\frac{\sigma_x}{P_{max}} = -(1+v)\left\{1 - \left(\frac{z}{c}\right)\left(\frac{a}{c}\right)\right\} + \frac{1}{2}\left(1 + \frac{z^2}{c^2}\right)^{-1} \quad (2)$$

$$\frac{\sigma_z}{P_{max}} = -\left(1 + \frac{z^2}{c^2}\right)^{-1} \quad (3)$$

Specific lubrication film thickness calculation

$$\tau = \frac{\sigma_x - \sigma_z}{2} \quad (4)$$

The thickness of the lubricant film that separates two surfaces plays an important role that depends on a few factors, notably the oil's viscosity, which varies with both temperature and pressure and surface roughness. The specific lubricant film thickness (λratio) is the parameter which is used to identify the lubricant working regimes such as boundary lubrication, mixed lubrication, elasto-hydrodynamic and hydrodynamic lubrication. It is defined as the ratio of the film thickness (h_0) divided by the composite surface roughness of the two surfaces that are separated by the fluid film defined in equation 5 [17].

R_1 and R_2 are the surface roughness of the contacting bodies. The minimum film thickness h_0 can be found out by the Dowson- Higginson relation defined in [18].

$$\lambda_{ratio} = \frac{h_0}{\sqrt{R_1^2 + R_2^2}} \quad (5)$$

Rolling contact fatigue testing

Rolling contact fatigue test is performed in a two roller-single cylinder standard test rig. The schematic of the rig is shown in Fig. 2(a). The test rig comprises two larger rollers of outer diameter 180 mm and a nose radius of 6.35 mm. The arrangement for holding the specimen is made by using a collect in the range of 10- 15 mm and is connected to a high-speed motor having a maximum speed capacity of 24000 rpm. Both the rollers are connected with a load cell, and the pneumatic actuator aids to control the load applied to the specimen. A speed sensor is placed near the specimen and a vibration sensor placed near one of the roller discs to measure the vibration level. A small lubricant tank with a lock and nut control system situated above the specimen so that the proper amount of lubricant can reach the contact point of the roller and specimen. The two discs along with the cylindrical specimen constitutes an elliptical hertzian contact schematically depicted in Fig. 2(b)
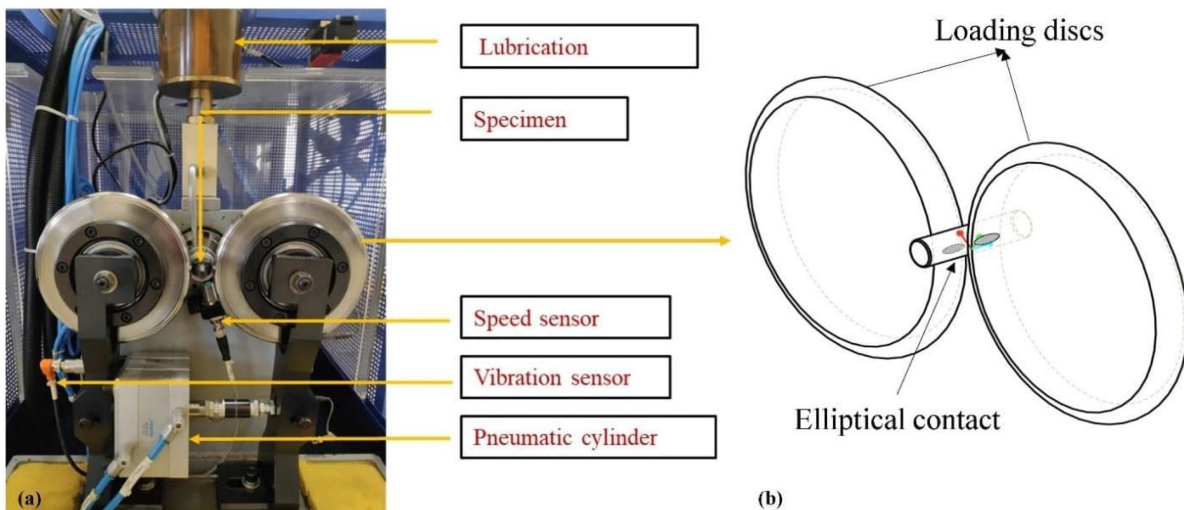
Fig.2: Disc on cylinder test rig (b) Schematic of the Hertzian elliptical contact

Table 2: Testing parameters

Parameter	value
Load	1.3 kN
Speed	12500 rpm
Contact pressure	4.47 GPa
λ_{ratio}	0.3- 1
Slip	0 %
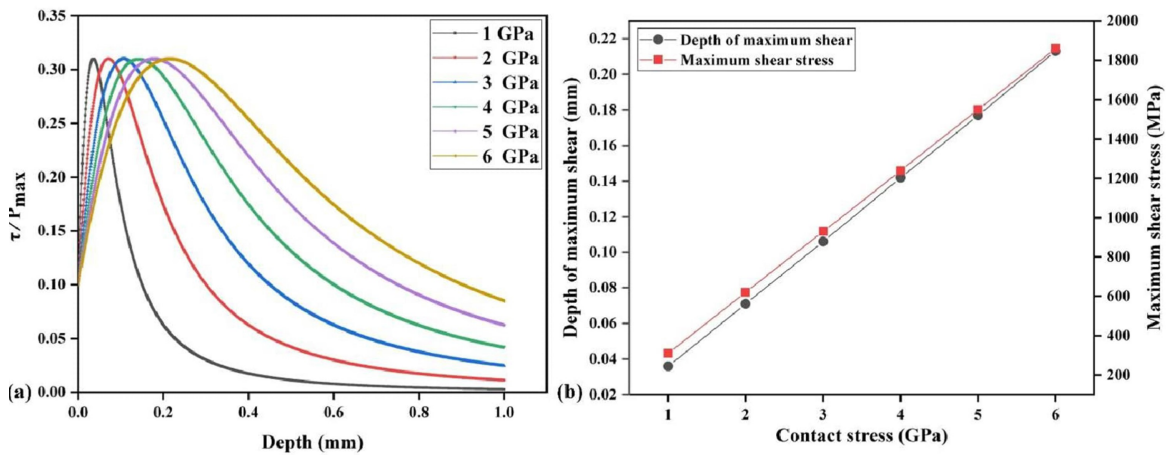
Fig. 3. (a) variation of shear stress on z-axis with contact pressure (b) variation of shear stress and depth of maximum shear stress with different contact pressures.

Testing conditions

Rolling contact fatigue tests were carried out on a two-disc single motor test rig under a mixed lubrication condition. The experimental parameters used for the test are listed below in Table 2.

Auto termination of the experiment is according to the vibration value of 10g (g- acceleration due to gravity) set on the machine. Most of the tests terminated by the formation of a pit on the contacting surface.

RESULTS AND DISCUSSION

Subsurface stress analysis

The normal and shear stress distribution at the contact is analyzed by FEM and the results are compared with the values obtained analytically. The analytical equations used to compute all contact parameters taken from [16]. For all the applied loads, the maximum shear region is always formed at the subsurface and the area of the stress region

increases with increase in applied load shown in Fig. 3a. The maximum value of shear stress is formed below the contact surface. The magnitude of shear stress and the depth at which maximum shear stress acting will be increased with an increase in applied load depicted in Fig. 3b.

The variation of major and minor axis of the elliptical contact (3D) is seen to be increased with increasing pressure seen in Fig. 4. It is interesting to note that the values of the major and minor axis are seen close by at lower contact stress. As the contact pressure increases, the variation is found to increase significantly.

Fig .5 shows that the contact pressure generated at the surface due to static load of 1.3 kN. The maximum pressure reached is 4.475 GPa at 1.3 kN, which relatively matches with the analytically calculated value of 4.42 GPa. The obtained profile of the contact pressure distribution is elliptical in shape and confirmed with Hertzian contact theory for non-conformal contact [19].

The values of semi major and semi minor axes are 0.3 mm and 0.4 mm shown in Fig. 5, as well as matches with analytical values of 0.3 mm and 0.36 mm respectively. The subsurface stresses for the Hertzian point contact were
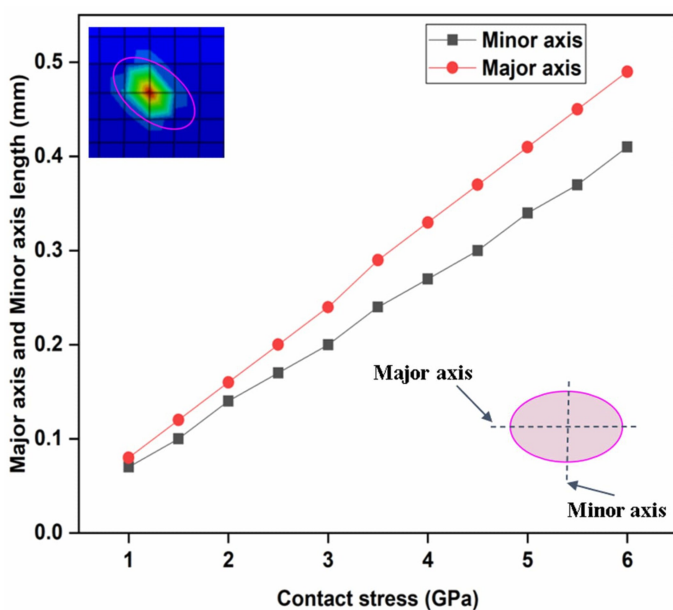
Fig. 4. Variation of elliptical axes with contact pressure.
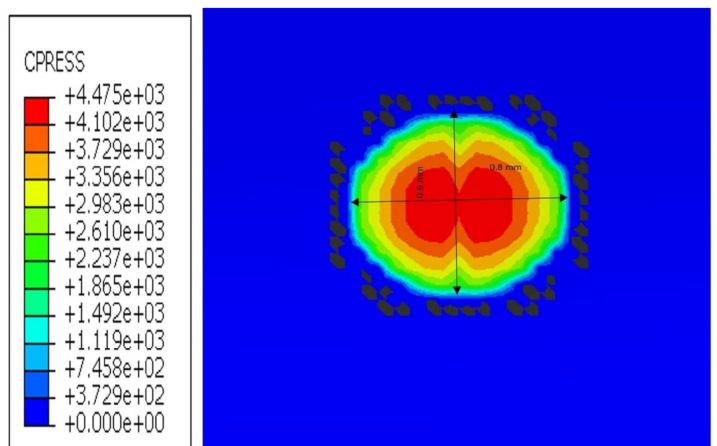
Fig. 5. Distribution of contact pressure on the surface of contact.
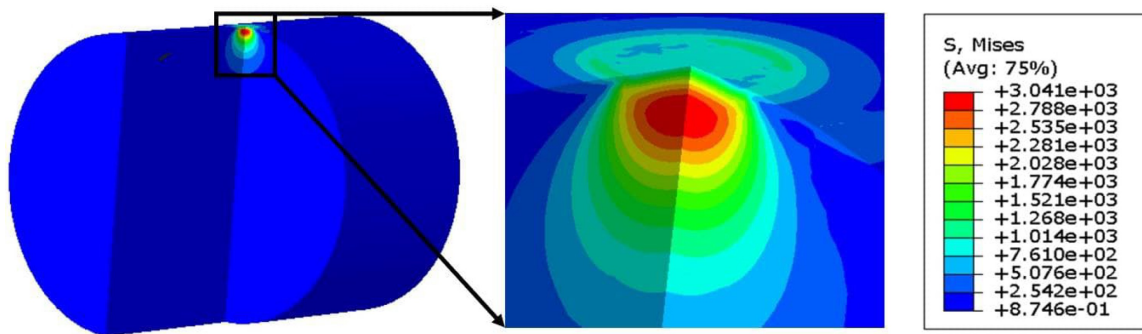
Fig. 6. Distribution of maximum subsurface shear stress due to applied static load of 1.3 kN.
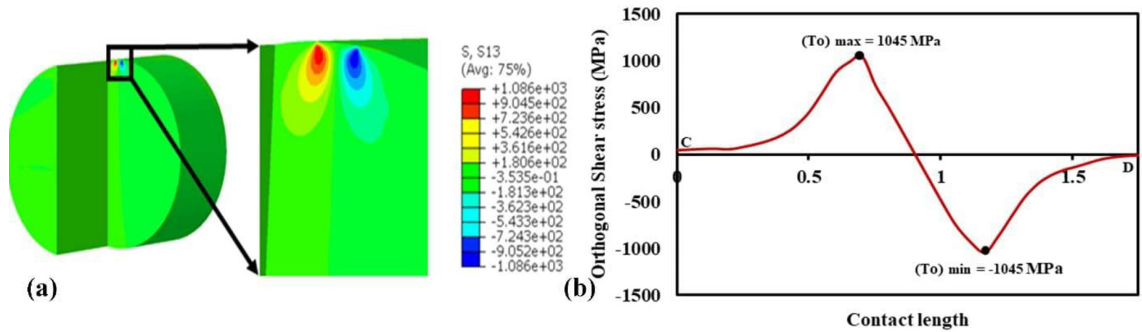
Fig. 7. (a and b) orthogonal shear stress distribution and its variation during static load.

determined for material properties listed in Table 1. Fig. 6 illustrates the subsurface shear stress contours for the point contact pressure distribution.

Fig .7 depicts that the shear stress reaches its maximum value at a distance of 0.15 mm below the contact surface as per the Hertzian contact theory.

The orthogonal shear stress developed at normal and parallel to contact surface region. These shear stresses appear at three different planes such as τ_{xy}, τ_{zx} and τ_{yz} in all of which maximum value is observed below the surface. However, the contact geometry will be the important factor in deciding a significant τ_{max} value and their respective plane. In this case the maximum τ_{max} value lies in the xz plane since the long-half width is perpendicular to the rolling direction and short-half width of the contact is oriented along the rolling direction. The maximum value of τ_{max} is located at 0.154 mm below the surface of contact. During the full load condition, the material undergoes completely reversed cyclic stress from τ_{max} of 1045 MPa and τ_{min} of -1045 MPa.

Effect of shot peening on the surface

As seen in Fig.8, the optical profilometry of the specimen surface before and after shot peening demonstrates a significant change in their topography. The surface with no shot peening contains only shallow channels and tiny pits that are formed during the machining process depicted in Fig. 8a. The surface roughness value for the same surface obtained was 84.12 nm. Shot Peening for 15 minutes raises the average surface roughness to 94.21 nm. More lands and microcavities are built upon increasing the shot peening duration to 30 minutes and the average surface roughness value increased

by 514.81 nm depicted in Fig. 8(b). Even though the surface irregularities detrimental to fatigue performance [20] it has been reported that the surface irregularity like lands and microcavities formed during shot peening process can act as lubricant reservoirs and, the lubricant emitted from such reservoirs increases the film thickness between the contacts [21]. It has been reported that the surface topographical changes (surface irregularities) show negative effects predominantly during "elastic hydrodynamic" lubrication due to larger pressure fluctuations at the contact surface. However, topographical changes have a favourable impact on RCF performance when asperity interactions occur, as in the mixed and boundary lubrication regimes. At these regimes, lubricant produced by micro-dents can successfully lift off the real roughness characteristics, reducing asperities interactions [22].

Hardness analysis

The cross section of the specimen is collected for the examination of the surface and subsurface hardness to identify the variation in hardness according to the shot peening time. The data in Fig.9 show that a progressive rise in surface hardness is observed as shot peening duration is increased. The material exhibits an average surface hardness value of 600 HV without shot peening. The highest surface hardness was obtained for 30 minutes of shot peening (710 HV) as compared to the 10-minute shot peened specimen (652 HV).

RCF Life

The boxplot in Fig. 10 shows the average RCF life calculated from three sets of experiments. It can be seen that when shot peening duration increases, the cycle to
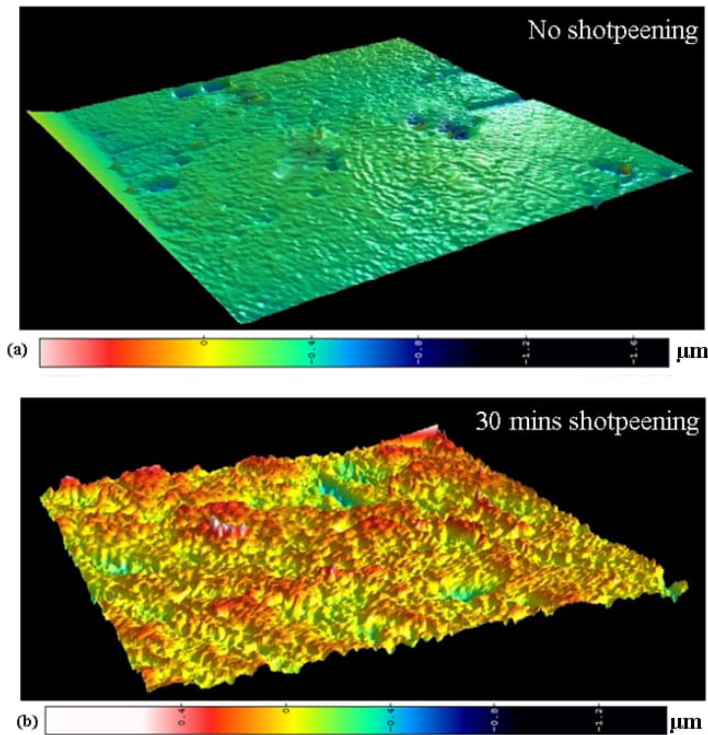
Fig. 8. Surface profiles of the specimen (a) before and (b) after shot peening
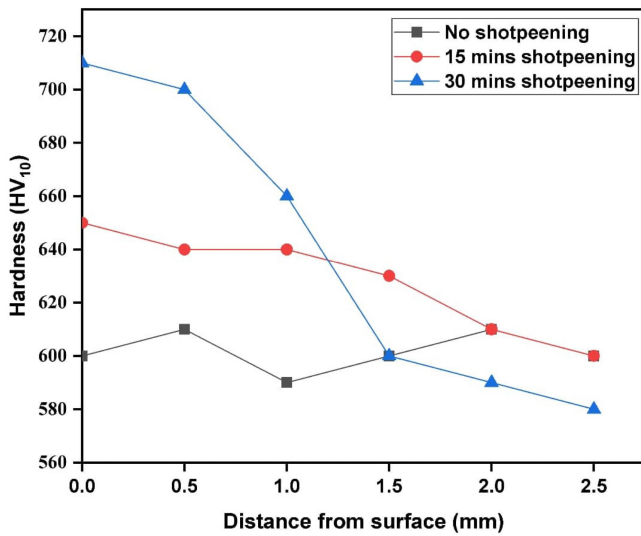
Fig. 9. Hardness profile of the shot peened specimens for different duration of time

failure also increases. An average RCF life of 1.15 million cycles is shown by the sample without shot peening. When the specimen was shot for 15 minutes, the RCF life was not found to significantly increase. However, almost 2-fold improvement in life is observed when the shot peening duration is increased to 30 minutes.

Taken together, these results suggest that the duration of the shot peening process and its impact on RCF life are considerable. Although the RCF life of the shot peened samples (30 minutes) is better than the non-shot peened specimen, the extent of the improvement varies depending on how long the shot peened specimen has been exposed
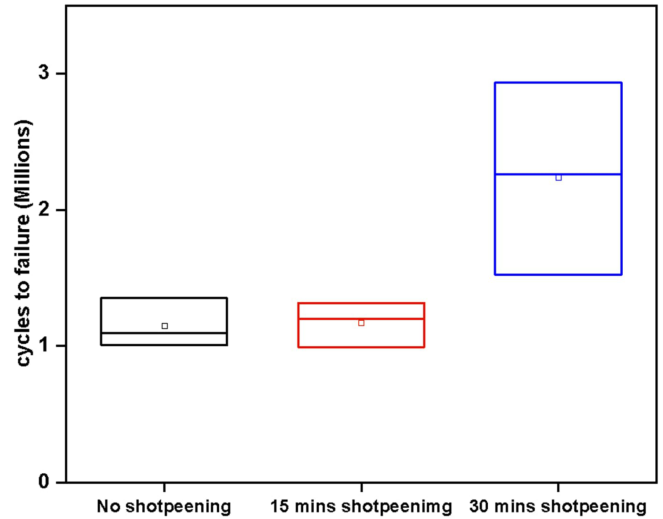
Fig. 10. Variation cycles to failure for shot-peened samples with time

to the shot. This might be as a result of the hardness increment variance depending on how long the shot peening process takes. Another explanation for this improvement in RCF life is the generation of compressive residual stress on the surface and in the vicinity of the surface during the shot peening process [8]. These induced compressive residual stresses tend to close the fatigue cracks formed and delays its propagation [22,23]. The additional microcavities created during the 30-minutes shot peening process is also one of the possible reasons to enhance the RCF performance in such a way that it can act as the lubrication reservoirs and delays lubricant film breakage. Previous studies reported that the lubricant released by shallow micro cavities can contribute to a temporary increase in film thickness, and consequently lowers the possibility of asperity interaction. The same study also revealed that the lapping process after shot peening process, eliminates the asperity peaks which in turn reduces the chances of asperity interaction as well as the internal stresses induced by the asperity contacts [21].

Subsurface crack analysis

A detailed subsurface crack analysis was performed in order to comprehend the crack origin and its propagation in line with stress distribution over surface and subsurface. Since the FEA analysis does not account for the hardness change caused by the shot peening process, a non-shot peened specimen is chosen for the subsurface crack investigation. Fig. 11a depicts the schematic of the failed specimen and the cross-section of it via the centre of the pit used for the subsurface examination. SEM images of a surface pit are shown in Fig. 11b, the pit's typical size ranges from 600 to 750 μm, and its depth ranges from 20 to 60 μm. The major surface and subsurface cracks propagate and connect before they spall at the subsurface at a depth of 165.5 microns as seen in Fig. 11c. Minor subsurface cracks origin then seen branching out and spreading further were observed.

From the plot (Fig. 7), it is clearly observed that the
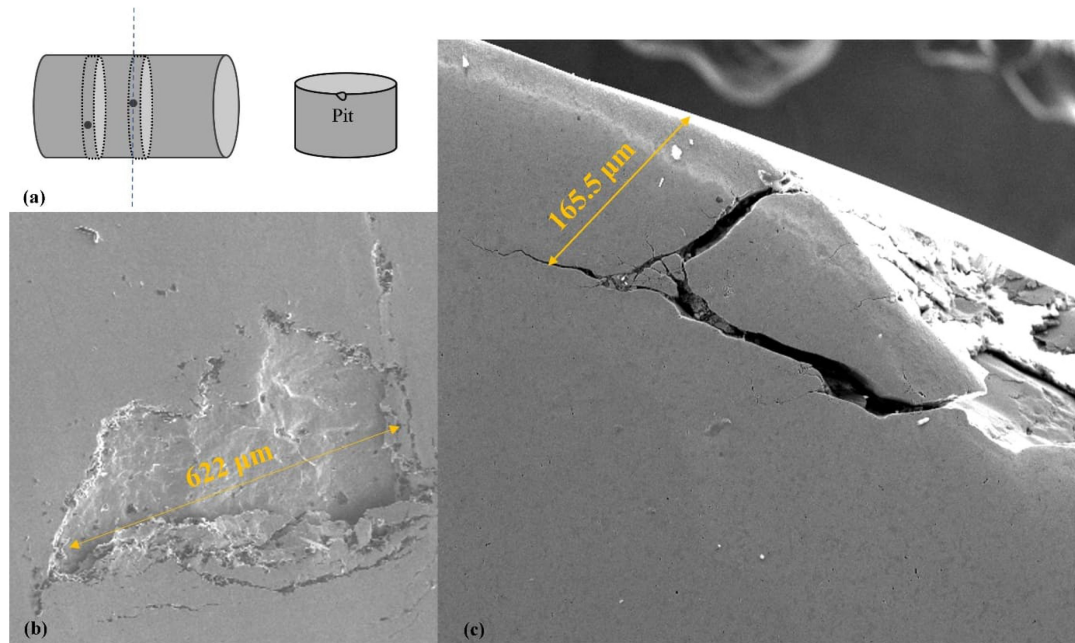
Fig. 11: (a) Schematic of the failed specimen by pit formation (b) cross section of the pit taken for microscopy (c) SEM image of the subsurface crack.

maximum value of shear stress is observed at the subsurface at a depth of 154 microns below the surface. The maximum shear stress region from the Fig.7 shows a good agreement with the subsurface crack network region obtained from the experimental studies (Fig.11). This maximum value of subsurface shear stress may be the reason for the origin or branching of the subsurface crack.

CONCLUSION

Experimental studies were conducted to study the effect of shot peening treatment on the RCF life of the EN3 31 steel. The shot peening process and its duration significantly impact rolling contact fatigue life. Shot Peening process increases the hardness of the material, leading to significant RCF life improvement. The period of 30 minutes shot peening increased hardness by 20.33%- and 10-minutes shot peening increased by 10.16% and also showed better fatigue life than no-shot peened specimens. shot peening for a shorter duration (10 minutes) doesn't give a significant improvement in RCF life, and that of longer shot peened specimen (30 minutes) shows a significant life improvement. The subsurface crack network region obtained from the experiential result significantly matches the maximum shear region obtained from the analytical and simulation calculation

Future work:

- Effect of contact pressure and rotational speeds on the rolling contact fatigue performance of a shot peened EN31 steel
- Effect of shot peening intensity on rolling contact fatigue life of EN 31 steel

REFERENCES

[1] Tedric A. Harris Michael Kotzalas. Essential Concepts of Bearing Technology. 2021. https://doi.org/10.1163/9789004447707_003.

[2] Tamada K, Tanaka H. Occurrence of brittle flaking on bearings used for automotive electrical instruments and auxiliary devices. Wear 1996;199:245–52. https://doi.org/10.1016/0043-1648(96)06990-6.

[3] Romanowicz PJ, Szybiński B. Fatigue life assessment of rolling bearings made from AISI 52100 bearing steel. Materials (Basel) 2019;12. https://doi.org/10.3390/ma12030371.

[4] Hoffmann G, Jandeska W. Effects on rolling contact fatigue performance-Part II. Gear Technol 2007;24:42–51.

[5] Turnia J, Sinclair J, Perez J. A review of wheel wear and rolling contact fatigue. Proc Inst Mech Eng Part F J Rail Rapid Transit 2007;221:271–89. https://doi.org/10.1243/0954409JRRT72.

[6] Manieri F, Stadler K, Morales-Espejel GE, Kadiric A. The origins of white etching cracks and their significance to rolling bearing failures. Int J Fatigue 2019;120:107–33. https://doi.org/10.1016/j.ijfatigue.2018.10.023.

[7] Mahdavi H, Poulios K, Kadin Y, Niordson CF. Finite element study of cyclic plasticity near a subsurface inclusion under rolling contact and macro-residual stresses. Int J Fatigue 2021;143:105981. https://doi.org/10.1016/j.ijfatigue.2020.105981.

[8] Klotz T, Delbergue D, Bocher P, Lévesque M, Brochu M. Surface characteristics and fatigue behavior of shot peened Inconel 718. Int J Fatigue 2018;110:10–21. https://doi.org/10.1016/j.ijfatigue.2018.01.005.

[9] Bhuvaraghan B, Srinivasan SM, Maffeo B, McClain RD, Potdar Y, Prakash O. Shot peening simulation using discrete and finite element methods. Adv Eng Softw 2010;41:1266–76. https://doi.org/10.1016/j.advengsoft.2010.09.003.

[10] Schulze V. Characteristics of Surface Layers Produced by Shot Peening. Shot Peen 2006:143–60. https://doi.org/10.1002/3527606580.ch20.

[11] Agaram S, Srinivasan SM, Kanjarla AK. Crystal plasticity modelling of stability of residual stresses induced by shot peening. Int J Mech Sci 2022;230:107526. https://doi.org/10.1016/j.ijmecsci.2022.107526.

[12] Bag A, Delbergue D, Ajaja J, Bocher P, Lévesque M, Brochu M. Effect of different shot peening conditions on the fatigue life of 300 M steel submitted to high stress amplitudes. Int J Fatigue 2020;130:105274. https://doi.org/10.1016/j.ijfatigue.2019.105274.

[13] Vantadori S, Valeo JV, Zanichelli A. Fretting fatigue and shot peening: a multiaxial fatigue criterion including residual stress relaxation. Tribol Int 2020;151. https://doi.org/10.1016/j.triboint.2020.106537.

[14] Pandey R, Deshmukh M. Shot peening and its impact on fatigue life of engineering componets. Int Conf Shot Peen Blast Clean 2001:1–20.

[15] Dassault Systèmes Simulia. Abaqus CAE User's Manual (6.12). Manuals 2012:1174.

[16] K L. Johnson. Contact mechanics. London: Cambridge university press; 1985.

[17] Stachowiak GW, Batchelor AW. Engineering tribology. 2005.

[18] D. Dowson G. H. Elasto- Hydrodynamic lubrication. vol. 23. first. Pergamon,1977; n.d.

[19] Nagarajan VR, Putatunda SK, Boileau J. Fatigue crack growth behavior of austempered AISI 4140 steel with dissolved hydrogen. Metals (Basel) 2017;7. https://doi.org/10.3390/met7110466.

[20] Klotz, T.Delbergue, D.Bocher, P. Lévesque, M. Brochu, M. Surface characteristics and fatigue behavior of shot peened Inconel 718. International Journal of Fatigue 2018:110:10-21.

[21] Vrbka M, Křupka I, Svoboda P, Šperka P, Návrat T, Hartl M, et al. Effect of shot peening on rolling contact fatigue and lubricant film thickness within mixed lubricated non-conformal rolling/sliding contacts. Tribol Int 2011;44:1726–35. https://doi.org/10.1016/j.triboint.2011.06.019.

[22] Krupka, I., Hartl, M. and Svoboda, P., 2010. Effects of surface topography on lubrication film formation within elastohydrodynamic and mixed lubricated non-conformal contacts. Proceedings of the Institution of Mechanical Engineers, Part J: Journal of Engineering Tribology, 224(8), pp.713-722.

[23] Zammit A, Mhaede M, Grech M, Abela S, Wagner L. Influence of shot peening on the fatigue life of Cu-Ni austempered ductile iron. Mater Sci Eng A 2012;545:78–85. https://doi.org/10.1016/j.msea.2012.02.092.

[24] Xiao H, Chen Q, Shao E, Wu D, Chen Z, Wang Z. The effect of shot peening on rolling contact fatigue behaviour and its crack initiation and propagation in carburized steel. Wear 1991;151:77–86. https://doi.org/10.1016/0043-1648(91)90347-W.